Acta Cryst. (1988). A44, 954-960

Dynamical Diffraction Effects on High-Resolution Electron Microscopy of Ordered Alloys

BY D. SHINDO AND M. HIRABAYASHI

Institute for Materials Research, Tohoku University, Sendai, Japan

(*Received* 19 *February* 1988; *accepted* 22 *June* 1988)

Abstract

Characteristic dynamical diffraction effects on high-resolution electron microscopy of perfectly and imperfectly ordered alloys are discussed using the multislice dynamical scattering theory. In contrast with short-range-ordered alloys, the scattering amplitude of the superlattice reflections of long-range-ordered alloys can be represented by a multiplication of the kinematical structure factor and the dynamical factor. It is shown that the dynamical factor does not depend on the ordered atomic arrangements, so the dynamical diffraction effect on the scattering amplitude of the superlattice reflections and also on the high-resolution superstructure images can be estimated through the dynamical factor as far as the alloy composition and the basic structure are known. The dynamical factor for Cu_3Pd is calculated as a function of crystal thickness and reciprocal-lattice vector.

1. Introduction

High-resolution electron microscopy (HREM) is a powerful technique for investigating structural defects in various materials (Spence, 1981; Fujita & Hirabayashi, 1986). In a series of high-voltage high-resolution electron microscopy (HVHREM) studies of alloys, several new long-period antiphase structures (Hiraga, Shindo, Hirabayashi, Terasaki & Watanabe, 1980; Terasaki, Mikata, Watanabe, Hiraga, Shindo & Hirabayashi, 1982) and related structural defects (Hiraga, Hirabayashi, Terasaki & Watanabe, 1982) have been revealed. The success of HVHREM in structural analyses of these alloys has been based on the one-to-one correspondence between the observed images and the projected ordered atomic arrangements. For example, in A_3B- or A_4B-type ordered alloys having the basic f.c.c. structure, B atom columns appear as white or black dots in the high-resolution images. It was thus possible to interpret directly the ordered atomic arrangement of the B atom sites in the f.c.c. structure. This one-to-one correspondence between the images and the ordered atomic arrangements has been explained theoretically on the basis of the dynamical diffraction theory in the real-space representation (Van Dyck, Van Tendeloo & Amelinckx, 1982) and also in terms of the kinematical relationship among the superlattice reflections in reciprocal space (Shindo, 1982).

Furthermore, in HVHREM studies of alloys having partially disordered atomic arrangements, it was shown that the high-resolution images can show the projected atomic arrangement in the alloys under well defined conditions (Shindo, Hiraga & Hirabayashi, 1984). Even in a more random state, very small microdomains of ordered structures were detected (Van Tendeloo & Amelinckx, 1985; Lee, Hiraga, Shindo & Hirabayashi, 1988). On the other hand, in HVHREM of perfectly ordered alloys based on the h.c.p. structure, strong dynamical diffraction effects were observed, and the image contrast was very sensitive to changes in crystal thickness (Shindo, Hiraga, Hirabayashi, Terasaki & Watanabe, 1983).

In this work, we systematically discuss the dynamical diffraction effects in imperfectly ordered as well as perfectly ordered alloys using the multislice dynamical theory (Cowley & Moodie, 1957; Cowley, 1981). An additional factor is introduced to represent the dynamical diffraction effect on the scattering amplitude. High-resolution images and the diffraction intensities are discussed in terms of the dynamical factor which is evaluated for Cu_3Pd.

2. General formulation of dynamical electron scattering in ordered alloys

In the following, we are mainly concerned with the scattering amplitude of superlattice reflections. This is because the high-resolution images which reflect the ordered atomic arrangements of alloys, called superstructure images, are, in general, directly produced by the superlattice reflections situated between the transmitted beam and the fundamental reflections (Fig. 1).

In order to evaluate the intensity distributions in both high-resolution images and electron diffraction patterns of ordered alloys including imperfectly ordered states, we consider dynamical electron diffraction based on the periodic continuation approximation for the structure whose unit cell is bounded by the artificial boundary shown in Fig. 2. The effect of this artificial boundary on the scattering amplitude can be neglected if the length of the unit cell, l, is large compared with the width of the boundary, Δl. With this artificial unit cell, the geometrically defined structure factor for the superlattice reflection

0108-7673/88/060954-07$03.00

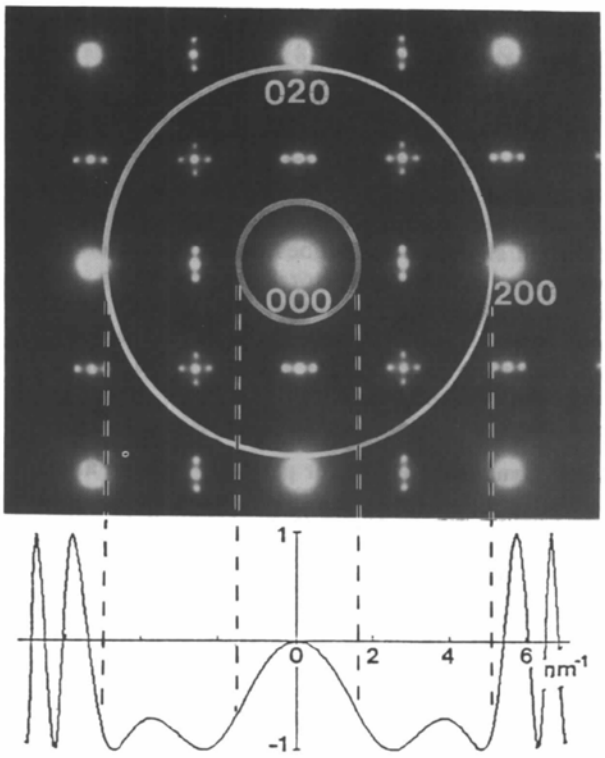

Fig. 1. Electron diffraction pattern of Cu–27 at.% Pd with a one-dimensional long-period superstructure, and the transfer function for a 1 MV electron microscope with $C_s = 11$ mm at the Scherzer condition. The passband of the transfer function is indicated by the concentric circles.

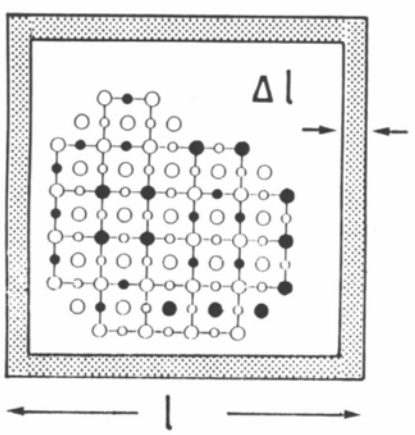

Fig. 2. Artificial unit cell assumed in the periodic continuation approximation for discussing dynamical electron diffraction in imperfectly ordered alloys.

u_j is given as

$$G(u_j) = \sum_i \gamma_i \exp(-2\pi i u_j r_i), \tag{1}$$

where γ_i is the occupation parameter

$$\gamma_i = \begin{cases} m_B \text{ for } A \text{ atom at } r_i \\ -m_A \text{ for } B \text{ atom at } r_i \end{cases}, \tag{2}$$

m_A and $m_B = (1 - m_A)$ being the atomic fractions of A and B, respectively. In considering the intensity distribution of high-resolution images, it is not necessary to set up such a large artificial unit cell, and we can use the column approximation instead.

According to the multislice theory (Cowley & Moodie, 1957; Cowley, 1981), the transmission function for superlattice reflections of the nth crystal slice is given by assuming the weak-phase-object approximation,*

$$Q_n^s(u) = \sum_j F(u) G_n(u) \delta(u - u_j), \tag{3}$$

where $\sum_j$ indicates a sum taken over all the superlattice reflections and

$$F(u) = i\sigma \Delta z T(u)[f_A(u) - f_B(u)], \tag{4}$$

$$G_n(u) = \sum_i \gamma_{in} \exp(-2\pi i u r_i). \tag{5}$$

In the above equations, σ, Δz and $T(u)$ are respectively the interaction constant, one crystal slice thickness and the temperature factor which we assumed to be isotropic. Δz is usually taken to be equal to the unit-cell length of a basic structure, *i.e.* 3–4 Å. f_A, f_B are the scattering factors of constituent atoms A and B. $G_n(u)$ is the geometrically defined structure factor for the nth crystal slice.

As previously adopted for perfectly ordered structures (Shindo, 1982), we assume two conditions for discussing dynamical diffraction effects in alloys, including imperfectly ordered ones:

$$|Q^f(H)| > |Q^s(h)| \tag{6}$$

$$G(h) = G(H + h), \tag{7}$$

where the one-dimensional representation is used for simplicity and H and h indicate the indices of fundamental and superlattice reflections, respectively. Since the structure factor of the fundamental reflection is assumed to be much larger than that of the superlattice reflection, we can neglect the scattering process from superlattice reflections into other superlattice reflections with the scattering vector corresponding to superlattice reflections. The condition (7) can be satisfied for ordered alloys based on the f.c.c. and b.c.c. structures. The general scattering amplitude of the superlattice reflection at a crystal

* In the case of alloys composed of heavy elements, a higher-order approximation should be applied, as shown later.

thickness $n\Delta z$ is given as

$$\begin{aligned}\Psi_n^s(H+h) &= \sum_{h_1} \Psi_{n-1}^f(H+h-h_1) \\ &\quad \times P(H+h-h_1)Q_n^s(h_1) \\ &\quad + \sum_{H_1} \Psi_{n-1}^s(H+h-H_1) \\ &\quad \times P(H+h-H_1)Q^f(H_1) \\ &= G_n(h)S_{n-1} + G_{n-1}(h)\sum_{H_1} S_{n-2}R_1 \\ &\quad + \ldots + G_{l+1}(h) \\ &\quad \times \sum_{H_1}\sum_{H_2}\cdots\sum_{H_{n-l-1}} S_l R_{n-l-1}\ldots R_2R_1 \\ &\quad + \ldots \\ &\quad + G_1(h)\sum_{H_1}\sum_{H_2}\cdots\sum_{H_{n-1}} S_0R_{n-1}\ldots R_2R_1, \end{aligned} \tag{8}$$

where

$$\begin{aligned}S_l &= \sum_{h_{n-l}} \Psi_l^f(H+h-H_1-H_2-\ldots-H_m-h_{n-l}) \\ &\quad \times P(H+h-H_1-H_2-\ldots-H_m-h_{n-l})F(h_{n-l})\end{aligned} \tag{9}$$

and

$$R_m = P(H+h-H_1-H_2-\ldots-H_m)Q^f(H_m). \tag{10}$$

In the above equations, P indicates the propagation function.

The product of S_l and G_{l+1} corresponds to the scattering from the fundamental reflection into the superlattice reflection $H+h$, and the multiplication of R_m indicates the scattering from the superlattice reflections with the scattering vector corresponding to fundamental reflections.

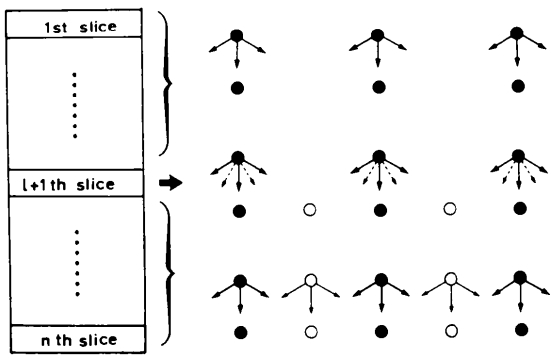

Fig. 3. Schematic illustration showing the dynamical scattering process represented in equation (11). See text for details. Full and open circles indicate fundamental and superlattice reflections, respectively. Arrows shown by solid and dotted lines show the scattering vectors corresponding to the fundamental and superlattice reflections, respectively.

As shown schematically in Fig. 3, the $(n-l)$th term in the right-hand side of (8),

$$G_{l+1}(h)\sum_{H_1}\sum_{H_2}\cdots\sum_{H_{n-l-1}} S_l R_{n-l-1}\ldots R_2R_1 \tag{11}$$

can be interpreted as the scattering amplitude of the superlattice reflection $(H+h)$ at the nth slice which is produced from the fundamental reflections at the $(l+1)$th slice and undergoes dynamical interactions with the scattering vectors corresponding to the fundamental reflections below the $(l+1)$th slice. The intensities of superlattice reflections and the contrast in high-resolution images are discussed below for different ordered states.

3. Dynamical factor for perfectly ordered alloys

As previously shown (Shindo, 1982), if the alloy is perfectly ordered, all the slices may have the same geometrical structure factor, *i.e.*

$$G_1(h) = G_k(h) \quad k = 2, \ldots, n, \tag{12}$$

then (8) is written in the simple form

$$\Psi_n^s(H+h) = G_1(h)E_n(H+h), \tag{13}$$

where

$$\begin{aligned}&E_n(H+h) \\ &\quad = \sum_{h_1} \Psi_{n-1}^f(H+h-h_1)P(H+h-h_1)F(h_1) \\ &\qquad + \sum_{H_1} E_{n-1}(H+h-H_1) \\ &\qquad \times P(H+h-H_1)Q^f(H_1) \quad \text{for } n>1, \\ &E_n(H+h) \\ &\quad = F(H+h) \qquad\qquad \text{for } n=1.\end{aligned} \tag{14}$$

In order to evaluate quantitatively the dynamical diffraction effect on the scattering amplitude of the superlattice reflections, we rewrite (13), comparing it to the kinematical expression (3) as

$$\Psi_n^s(H+h) = G_1(h)F(H+h)D_n(H+h), \tag{15}$$

where

$$D_n(H+h) = [F(H+h)]^{-1}E_n(H+h). \tag{16}$$

This shows that the scattering amplitude is simply given as a product of the kinematical structure factor and a 'dynamical factor'* $D_n(H+h)$, which is dimensionless and represents the dynamical scattering effect on the scattering amplitude.

It should be noted that the dynamical factor does not depend directly on the ordered atomic

* 'Dynamical factor' was introduced here for the scattering amplitude of superlattice reflections. The term called 'dynamical modulation' or 'dynamical factor' which has been used for describing the dynamical diffraction effect on diffuse scattering intensity (Fisher, 1965; Cowley & Pogany, 1968) will be mentioned in § 4.3.

arrangement, *i.e.* $G_1(h)$. Hence we can estimate the dynamical diffraction effect from knowledge of alloy composition. As an example, $D_n(h)$ for the long-period superstructure of Cu_3Pd which has been studied extensively by HREM (Broddin, Van Tendeloo, Van Landuyt, Amelinckx, Portier, Guymont & Loiseau, 1986; Takeda, Kulik, de Fontaine & Tanner, 1986) will be evaluated later. The intensity of superlattice reflections can be directly given from (15), *viz*

$$|\Psi_n^s(H+h)|^2 = |G_1(h)F(H+h)|^2 |D_n(H+h)|^2. \tag{17}$$

The contrast of high-resolution images can also be represented as

$$\begin{aligned} I(x) &= |\mathcal{F}[\Psi_n(0) + \Psi_n^s(h)]|^2 \\ &= |C + i\mathcal{F}[G_1(h)F(h)] * \mathcal{F}[D_n(h)]|^2 \\ &\qquad (C = \text{constant}), \end{aligned} \tag{18}$$

where $*$ indicates the convolution operation. In (18), perfect spatial and temporal coherence is assumed for the superlattice reflections situated between the transmitted beam and the fundamental reflections (Fig. 1). The contrast of the high-resolution image for a simple case,

$$D_n(h) = \text{constant}, \tag{19}$$

was discussed previously (Shindo, 1982). It was concluded that two types of interpretable images could be obtained depending on the relative amplitudes and phases of the transmitted beam and the superlattice reflections around it. The contrast of the first is represented directly by the potential difference of constituent atoms, *i.e.* $\pm\varphi_s(x)$, where the sign was determined by the relative phase of the superlattice reflections and the transmitted beam. The contrast of the other is proportional to the square of the potential difference, *i.e.*

$$|c\varphi_s(x)|^2 \quad (c = \text{constant}). \tag{20}$$

This is obtained when the transmitted beam is absolutely extinct at some crystal thickness. In both cases, we can directly correlate the contrast of high-resolution images with the ordered atomic arrangement. The above argument revealed that the potential difference $\varphi_s(x)$ which is reflected in the image intensity should generally be modulated by convolution with the Fourier transform of the dynamical factor, $\mathcal{F}[D(h)]$.

4. Dynamical factor for imperfectly ordered alloys

Following the above discussion, we will extend the dynamical scattering equation to imperfectly ordered alloys, in which the correlation of atomic arrangements extends to some limited range. We will discuss the dynamical electron diffraction effects for three different ordered states, homogeneous partial order, heterogeneous partial order and short-range order.

4.1. *Homogeneous partial order*

In a partially ordered structure, the long-range-order parameter is less than unity. When the disordering occurs homogeneously, the crystal may be divided into slices where each slice has the same crystal potential $\psi(x)$ projected along the incident electron beam. If there is a microscopic inhomogeneity due to the disordering, the slice is taken to be thicker than that of the unit-cell length of the basic f.c.c. or b.c.c. structure, and $\psi(x)$ should be written as a summation of the projected potentials $\varphi_j(x)$ over m ($m > 1$) slices whose thickness corresponds to the basic structure, *i.e.*

$$\psi(x) = \sum_{j=1}^{m} \varphi_j(x). \tag{21}$$

Since this projected potential may not be small enough to apply the weak-phase-object approximation for the transmission function, we have to use the approximation of higher order,

$$\begin{aligned} \exp[i\sigma\psi(x)] &= \exp\left\{ i\sigma\left[m\varphi(x) + \sum_{j=1}^{m} \Delta\varphi_j(x) \right] \right\} \\ &= \exp[i\sigma m\varphi(x)] \\ &\quad \times \left[1 + i\sigma \sum_{j=1}^{m} \Delta\varphi_j(x) + \ldots \right] \\ &\simeq \exp[i\sigma m\varphi(x)] \\ &\quad + \exp[i\sigma m\varphi(x)] i\sigma \sum_{j=1}^{m} \Delta\varphi_j(x). \end{aligned} \tag{22}$$

Fourier transformations of the first and the second terms on the right-hand side of (22) give the transmission function for the fundamental and the superlattice reflections, respectively. Thus the transmission function for the second term may be written in reciprocal space as

$$\begin{aligned} Q^s(H+h) &= \mathcal{F}\left\{ \exp[i\sigma m\varphi(x)] \left[i\sigma \sum_{j=1}^{m} \Delta\varphi_j(x) \right] \right\} \\ &= Q_m(H+h) * i\sigma \sum_{j=1}^{m} \mathcal{F}[\Delta\varphi_j(x)] \\ &= \sum_{h_1} Q_m(H+h-h_1) \left[F(h_1) \sum_{j=1}^{m} G_j(h_1) \right] \\ &= \sum_{j=1}^{m} G_j(h) \left[\sum_{h_1} Q_m(H+h-h_1) F(h_1) \right]. \end{aligned} \tag{23}$$

Replacing $G(h)$ in (3) by $\sum_{j=1}^{m} G_j(h)$ and $F(h)$ by $\sum_{h_1} Q_m(H+h-h_1)F(h_1)$, we can define the

dynamical factor as

$$D_n(H+h)=\left[\sum_{h_0} Q_m(H+h-h_0)F(h_0)\right]^{-1}$$
$$\times\left[\sum_{h_1}\Psi^f_{n-1}(H+h-h_1)P(H+h-h_1)\right.$$
$$\times\sum_{h_2} Q_m(H+h_1-h_2)F(h_2)$$
$$\left.+\sum_{H_1} D_{n-1}(H+h-H_1)P(H+h-H_1)\right.$$
$$\left.\times Q^f(H_1)\right] \quad \text{for } n>1,$$
$$D_n(H+h)=1 \qquad \text{for } n=1. \qquad (24)$$

Thus the dynamical diffraction effects in alloys with homogeneous partial order can be discussed with this dynamical factor in the same manner as the perfectly ordered alloys.*

4.2. *Heterogeneous partial order*

In contrast with § 4.1, we consider here the case when perfectly ordered microdomains coexist with the disordered matrix as shown in Fig. 4. If a perfectly ordered domain extends from the $(l+1)$th slice to the $(l+k)$th slice parallel to the incident electron beam and has the geometrical structure factor $G_0(h)$, then the scattering amplitude is written directly from (8) as

$$\Psi^s_n(H+h)=G_0(h)F(H+h)D_n(H+h), \quad (25)$$

where

$$D_n(H+h)=[F(H+h)]^{-1}\left[\sum_{H_1}\sum_{H_2}\cdots\sum_{H_{n-l-1}} S_l R_{n-l-1}\right.$$
$$+\ldots+R_2R_1+\ldots$$
$$\left.+\sum_{H_1}\sum_{H_2}\cdots\sum_{H_{n-l-k}} S_{l+k-1}R_{n-l-k}\ldots R_2R_1\right]. \qquad (26)$$

In the above equation, we neglect the scattering contribution from the disordered matrix, provided that the perfectly ordered microdomain is fairly large along the incident electron beam. In this simplest case, the dynamical diffraction effects on HREM can be represented using the dynamical factor (26) in the same way as described for the perfectly ordered alloy. Recently image simulations of this type of partial order were performed for the image interpretation of short-range-ordered alloys using the column approximation (Tanaka & Cowley, 1987). If the large ordered domains overlap in projection parallel to the incident electron beam, the dynamical diffraction effect cannot be evaluated with this type of dynamical factor.

* The weak-phase-object approximation may not be applied to the transmission function of ordered alloys composed of heavy elements. The higher-order approximation (22) should be applied in this case provided $m=1$.

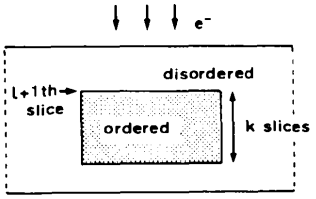

Fig. 4. A simple model with heterogeneous partial order. Perfectly ordered domain in the shaded region is surrounded by the disordered structure.

4.3. *Short-range order*

In a short-range-ordered state, the pair correlation of atoms becomes weaker as the pair distance increases. The statistical correlation of the atom pairs is usually characterized by the so called Warren-Cowley short-range-order parameter α_{ij}, which is given with the geometrical structure factor as

$$\alpha_{ij}=C\sum_i\sum_j \gamma_i\gamma_j$$
$$=C\sum_h |G(h)|^2\exp(2\pi ihx), \qquad (27)$$

where the geometrical structure factor can be defined for a large artificial unit cell (Fig. 2) to give the statistical correlation.

The pair correlation may be limited in a few slices in the electron beam direction, and so $G_n(h)$ changes from slice to slice. Simplification of the scattering amplitude (8) cannot be made in this case. However, the intensity of diffuse scattering can be given in terms of a factor which is similar to the dynamical factor introduced as above, assuming that the diffuse scattering from each slice is independent and uncorrelated,

$$|\Psi^s_n(H+h)|^2=|G_n(h)|^2|S_{n-1}|^2$$
$$+|G_{n-1}(h)|^2\left|\sum_{H_1} S_{n-2}R_1\right|^2$$
$$+\ldots+|G_1(h)|^2$$
$$\times\left|\sum_{H_1}\sum_{H_2}\cdots\sum_{H_{n-1}} S_0R_{n-1}\ldots R_1\right|^2$$
$$=C'\sum_i\sum_j \alpha_{ij}\exp[2\pi i(hx)]D'(H+h), \qquad (28)$$

where

$$D'(H+h)=\left[|S_{n-1}|^2+\left|\sum_{H_1} S_{n-2}R_1\right|^2+\ldots\right.$$
$$\left.+\left|\sum_{H_1}\sum_{H_2}\cdots\sum_{H_{n-1}} S_0R_{n-1}\ldots R_1\right|^2\right]. \qquad (29)$$

Thus the intensity of diffuse scattering in the short-range-ordered alloy is represented by the multiplication of the Fourier transforms of the short-range-order parameter and the factor $D'(H+h)$. This type of approximation was first introduced by Gjönnes (1965) in his general diffuse scattering theory and developed extensively by Fisher (1965), and Cowley and his colleagues (Cowley & Pogany, 1968; Cowley & Murray, 1968; Cowley & Fields, 1979).

5. Evaluation of dynamical factor

We evaluate the dynamical factor for perfectly ordered Cu_3Pd as a function of crystal thickness and reciprocal-lattice vector assuming the use of a 1 MV electron microscope. For the evaluation using (14) and (16), we must know the scattering amplitude of the transmitted beam and the fundamental reflections as a function of crystal thickness. We assume here disordered f.c.c. Cu_3Pd in the evaluation. In Fig. 5, the absolute value of the dynamical factor $|D_n(u)|$ is shown in reciprocal space for the crystal thickness $t = 0{\cdot}74$–$16{\cdot}7$ nm. It is interesting to note that the dynamical factor does not change much with the reciprocal-lattice vector, but it increases rapidly with the crystal thickness. In the crystal thickness range shown here, the superlattice reflections with higher indices tend to be excited more strongly.

In the evaluation of the dynamical factor in Fig. 5, we assumed that the scattering amplitudes of the transmitted beam and the fundamental reflections are not affected by the scattering from and into the superlattice reflections. In order to investigate validity of the above assumption, we compared the scattering amplitude of the disordered structure with that of a simple ordered structure of the $L1_2$ type. In Fig. 6, the amplitudes of the transmitted beam and the fundamental reflection 200 were calculated as a function of crystal thickness. In a crystal thicker than 8 nm, the scattering amplitudes from the disordered f.c.c. and $L1_2$ type structures differ considerably from each other. Hence if we investigate the dynamical diffraction effects on HREM of a long-period antiphase structure which is based on some simple ordered structure such as the $L1_2$ type, we must use the scattering amplitudes of the transmitted beam and the fundamental reflections calculated from the $L1_2$ type ordered structure instead of the disordered f.c.c. structure for evaluating the dynamical factor in crystals thicker than 10 nm.

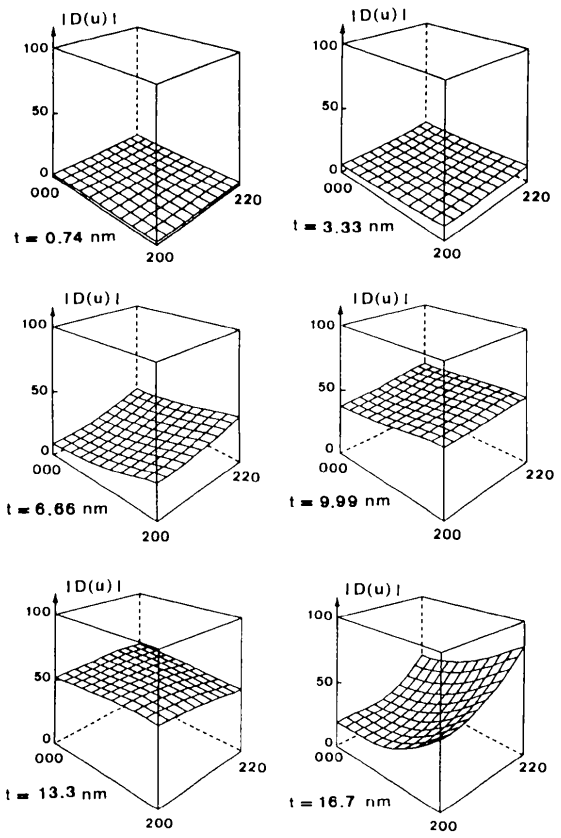

Fig. 5. Absolute value of the dynamical factor for Cu_3Pd assuming the use of a 1 MV electron microscope.

6. Discussion

Finally we discuss the conditions which were used to introduce the dynamical factor $D(h)$. The condition (7) for the geometrically defined structure factor can be satisfied when all the atom sites of the crystal slice projected along the incident electron beam form a two-dimensional primitive lattice containing one lattice point. For ordered alloys with the basic f.c.c. and b.c.c. structures, the above condition is satisfied, but not for alloys based on the h.c.p. structure, or imperfect crystals containing structural defects. In these cases, we cannot introduce the dynamical factor and no linear relationship holds between the scattering amplitude and the kinematical structure factor of the superlattice reflections. In practice, strong dynamical diffraction effects were observed on the scattering

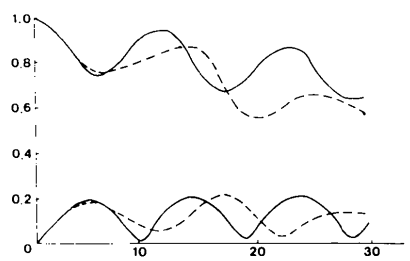

Fig. 6. Amplitude of the transmitted beam and the fundamental reflection 200 for Cu_3Pd as a function of crystal thickness. Solid and dotted lines are calculated values based on the disordered f.c.c. and $L1_2$ type ordered structures, respectively.

amplitude of the superlattice reflections of $Au_{77}Mg_{23}$ and $Au_{77}Cd_{23}$ which have a two-dimensional long-period antiphase structure based on the h.c.p. structure (Shindo, Hiraga, Hirabayashi, Terasaki & Watanabe, 1983). It was noticed that the contrast of the high-resolution images of these alloys changes sensitively with the crystal thickness.

In deriving the equation for the dynamical factor, we neglected double-weak scattering (Gjönnes, 1965; Spence, 1978) on the basis of condition (6), and assumed either the weak-phase-object approximation (3) or the similar approximation of higher order (23). These approximations can be more appropriately applied to alloys of which the constituent atoms have similar atomic scattering factors. We also note that the approximation holds to greater thickness for electron microscopy with higher accelerating voltages, because the interaction constant becomes smaller. In the limiting case, when a thin film of ordered alloy composed of elements with similar atomic numbers is examined with a high-voltage electron microscope, the dynamical factor tends to take a constant value for the superlattice reflections which contribute to the high-resolution images; so kinematical interpretation in HREM may be possible. It should be noted that the above argument can be applied to not only such simple ordered structures as discussed here but also complicated ones such as two-dimensional long-period antiphase structures which satisfy the conditions (6) and (7). This is because the dynamical factor does not directly depend on the ordered atomic arrangements.

The authors wish to thank Dr K. Hiraga for invaluable discussions. They also thank Dr T. B. Williams for useful comments on the manuscript.

References

BRODDIN, D., VAN TENDELOO, G., VAN LANDUYT, J., AMELINCKX, S., PORTIER, R., GUYMONT, M. & LOISEAU, A. (1986). *Philos. Mag.* **A54**, 395-419.

COWLEY, J. M. (1981). *Diffraction Physics.* 2nd revised ed. Amsterdam: North-Holland.

COWLEY, J. M. & FIELDS, P. M. (1979). *Acta Cryst.* **A35**, 28-37.

COWLEY, J. M. & MOODIE, A. F. (1957). *Acta Cryst.* **10**, 609-619.

COWLEY, J. M. & MURRAY, R. J. (1968). *Acta Cryst.* **A24**, 329-336.

COWLEY, J. M. & POGANY, A. P. (1968). *Acta Cryst.* **A24**, 109-116.

FISHER, P. M. J. (1965). *Proc. Int. Conf. Electron Diffraction and Crystal Defects*, paper IH-4. Melbourne: Australian Academy of Science.

FUJITA, F. E. & HIRABAYASHI, M. (1986). *Microscopic Methods in Metals*, edited by U. GONSER. Berlin: Springer-Verlag.

GJÖNNES, J. K. (1965). *Proc. Int. Conf. Electron Diffraction and Crystal Defects*, paper IH-2. Melbourne: Australian Academy of Science.

HIRAGA, K., HIRABAYASHI, M., TERASAKI, O. & WATANABE, D. (1982). *Acta Cryst.* **A38**, 269-274.

HIRAGA, K., SHINDO, D., HIRABAYASHI, M., TERASAKI, O. & WATANABE, D. (1980). *Acta Cryst.* **B36**, 2550-2554.

LEE, K. H., HIRAGA, K., SHINDO, D. & HIRABAYASHI, M. (1988). *Acta Metall.* **36**, 641-649.

SHINDO, D. (1982). *Acta Cryst.* **A38**, 310-317.

SHINDO, D., HIRAGA, K. & HIRABAYASHI, M. (1984). *Sci. Rep. Res. Inst. Tohoko Univ. Ser. A*, **32**, 32-45.

SHINDO, D., HIRAGA, K., HIRABAYASHI, M., TERASAKI, O. & WATANABE, D. (1983). *J. Appl. Cryst.* **16**, 233-238.

SPENCE, J. C. H. (1978). *Acta Cryst.* **A34**, 112-116.

SPENCE, J. C. H. (1981). *Experimental High-Resolution Electron Microscopy.* Oxford: Clarendon Press.

TAKEDA, S., KULIK, J., DE FONTAINE, D. & TANNER, L. E. (1986). *Proc. 11th Int. Congr. on Electron Microscopy*, edited by T. IMURA, S. MARUSE & T. SUZUKI, pp. 957-958. Kyoto: Japanese Society of Electron Microscopy.

TANAKA, N. & COWLEY, J. M. (1987) *Acta Cryst.* **A43**, 337-346.

TERASAKI, O., MIKATA, Y., WATANABE, D., HIRAGA, K., SHINDO, D. & HIRABAYASHI, M. (1982). *J. Appl. Cryst.* **15**, 65-71.

VAN DYCK, D., VAN TENDELOO, G. & AMELINCKX, S. (1982). *Ultramicroscopy*, **10**, 263-280.

VAN TENDELOO, G. & AMELINCKX, S. (1985). *Acta Cryst.* **B41**, 281-292.

Acta Cryst. (1988). A44, 960-965

A Top–Bottom Contrast Effect in Dark-Field Images Arising from *N*-Beam Dynamic Refraction

BY F. FUJIMOTO

College of General Education, University of Tokyo, Komaba, Megura, Tokyo 153, *Japan*

AND P. GOODMAN

School of Physics, University of Melbourne, Parkville, Australia 3052

(*Received* 7 *December* 1987; *accepted* 22 *June* 1988)

Abstract

The refraction effect associated with an off-Bragg diffracted beam in high-energy transmission electron diffraction is analysed. It is found that the wave vectors of Bloch-wave components of a beam associated with a finite excitation error are significantly shortened or lengthened as a consequence of dynamic scattering, with the direction of change being determined by the sign of the excitation error. By

0108-7673/88/060960-06$03.00